

# Constitutive modeling of residual soils based on irreversible strains decomposition

Alessandro Cirone<sup>1,#</sup> , Eurípedes Vargas Jr.<sup>1</sup> , Tácio de Campos<sup>1</sup> 

Article

## Keywords

Constitutive relations  
Plasticity  
Residual soil

## Abstract

A constitutive model is proposed for describing the stress-strain behavior of saturated residual soils based on experimental observations from oedometer testing, triaxial and direct shear testing. The model is formulated within the classical theory of plasticity with a non-associated flow rule. In order to reproduce particular features of residual soils, inelastic strains are decomposed in two components, namely the plastic dilation due to the rearrangement of grains and the volumetric collapse resulting from bonds degradation. The yield surface is tear-drop shaped and obeys an isotropic volumetric strain-hardening rule related to collapse strains, along with a shear softening with developing plastic deviatoric strains. Comparison with published experimental data confirms the capability of the model of reproducing observed behavior of tropical residual soils in consolidated drained and undrained triaxial compression.

## 1. Introduction

The term residual soil is widely used in contrast to *sedimentary (or transported) soil* to designate those soils that do not derive from erosion, transport and deposition of sediments, but result substantially from the in place weathering of the parent rock (Duarte & Rodrigues, 2017). This origin-based definition reflects the importance of lithological characteristics and environmental conditions on the engineering behavior of residual soils, whose description and study cannot be dissociated from the respective weathering history of the parent rock.

Occurring in many regions of Brazil, residual soils may derive from the weathering of granite, gneiss, basalt or sandstone. In southern Brazil residual soils from basalt are dominant (Consoli et al., 1998), whereas weathering profiles of granite-gneiss are commonly encountered around São Paulo and Rio de Janeiro (de Mello, 1972). Martins et al. (2005) have also reported a residual soil originated from the weathering the Aeolian Botucatu sandstone.

The weathering profile reflects the decay of rock towards the residual soil condition. Typical examples from Brazilian literature have been reported by Viana da Fonseca & Coutinho (2008). Ideally, the weathering profile consists of different horizons varying from sound rock, weathered rock to residual soil. If the soil exhibits features from the parent rock, then it is classified as *young residual*

*soil* or *saprolitic soil*. Otherwise, if there is no detectable relic structure, the expression *mature residual soil* is used. On top, one may encounter *lateritic* soils or transported soils (*colluvium*) that may undergo weathering as well. Lateritic soils contains laterite, which is impregnated with, cemented by or partly replaced by hydrated oxides of iron and aluminium (Fookes, 1997). Quite well known by Brazilian engineers, these denominations were further explained by Vargas (1953) and Barata (1969).

Depending on the weathering grade, residual soils may preserve macrostructure inherited from the parent rock (schistosity, fissures, joints, litho-relicts etc.) as well as microstructure (macropores, fabric, bonds between particles). According to Costa Filho et al. (1989), the presence a weakly bonded structure, resulting from predominant chemical weathering, provides to the residual soil:

- true cohesion in terms of effective stress
- apparent preconsolidation pressure related to structure and bonds strength
- higher stiffness at lower stresses and plastic behavior at higher stresses, characterizing a yield surface.

The natural process of weathering influences the composition (clay minerals), grain shape, grain size, void ratio, structure, permeability, strength and deformability of residual soils. Obviously, those features strongly affect the overall engineering behavior of residual soils, as well explained in the general reports provided by Blight (1989)

<sup>#</sup>Corresponding author. E-mail address: acirone@puc-rio.br.

<sup>1</sup>Departamento de Engenharia Civil e Ambiental, Pontifícia Universidade Católica do Rio de Janeiro, Rio de Janeiro, RJ, Brazil.

Submitted on May 15, 2020; Final Acceptance on August 5, 2020; Discussion open until March 31, 2021.

DOI: <https://doi.org/10.28927/SR.434647>



This is an Open Access article distributed under the terms of the Creative Commons Attribution License, which permits unrestricted use, distribution, and reproduction in any medium, provided the original work is properly cited.

and Costa Filho et al. (1989). From a mechanical standpoint, weathering is modeled as a softening process (Vaughan & Kwan, 1984).

During the last four decades an extensive laboratory work has been carried out mainly at Rio de Janeiro to study the stress-strain relationships of tropical granite-gneiss residual soils. Testing has been carried out on intact and compacted samples of local lateritic and saprolitic soils, under both saturated and unsaturated conditions. Strong experimental evidences have been produced and some patterns of the geotechnical behavior have been established. The research focused mostly on the geotechnical and geological characterization, analyzing test results according to the conventional principles and methods of soil and rock mechanics. Similar studies have been carried out on residual soils from the São Paulo Metropolitan Area (Futai et al., 2012), North-east of Argentina (Bogado et al., 2019; Francisca & Bogado, 2019), Indonesia and New Zealand (Wesley, 2009) and Hong Kong (Rocchi & Coop, 2015), just to cite a few.

The experimental characterization has been accompanied by the need of developing a modeling framework for predicting the mechanical behavior of residual soils and the response of related geotechnical structures. Various advanced constitutive models have been employed and tested. Some researchers used enhanced versions of Cam Clay, introducing isotropic damage (Puppi et al., 2018), influence of structure (Mendoza et al., 2014) or the subloading surface (Mendoza & Muniz de Farias, 2020). Others (Azevedo et al., 2006) have used the Lade's model (Lade & Kim, 1988; Kim & Lade, 1988) and the discrete element modeling approach (Ibañez, 2008). Unfortunately, most of the aforementioned models were conceived for sedimentary soils and then adjusted to residual soils. In contrast, the authors have developed a constitutive model specifically designed to reproduce the behavior of residual soils starting from experimental observations. The main assumption is the decomposition of irreversible strains into two mechanisms: the particle rearrangement and the bonds degradation. In addition, specific hardening laws have been adopted.

This paper presents the formulation of this new constitutive model within the framework of classical strain hardening plasticity. In doing so, the behavior of saturated residual soils observed from oedometer testing, triaxial and direct shear testing is firstly examined. Then, the constitutive model is formulated and validated in drained and undrained triaxial compression tests.

## 2. Shear strength and stress-strain behavior of residual soils

For sake of clarity, results of several tests on residual soils are herein summarized to establish patterns of the behaviour observed from oedometer testing, triaxial and direct shear testing.

Figure 1 presents the results of a  $K_0$ -test on a partially saturated sample of intact gneissic residual soil carried out by Maccarini (1980, 1987). The sample was obtained from the slope of an excavation at a depth of 8.05 m, measured from the original ground level, where the total vertical in situ stress was estimated to be 130 kPa prior the excavation. The sample was incrementally loaded under stress control allowing drainage from top and bottom against atmospheric pressure.

As shown in Figure 1(a), below a quite pronounced yield stress,  $\sigma_{vm}$ , located around 200-250 kPa, the behavior is stiff and elastic. This first part of the oedometric curve comprises a reloading stage. As the vertical stress is increased, yield occurs, the soil becomes more compressible and the behavior is elastoplastic. This is reflected by the sharp difference of the slopes in the compression curve of Figure 1(a). Figure 1(b) shows that the same trend is clearly followed by the stress path in the  $(q, p)$  plane. There is an initial elastic response and stress path draws a straight line up to the yield stress. Further loading deviates the stress path, which gradually approaches the  $K_0$ -line of the destructured soil (Leroueil & Vaughan, 1990) as the vertical stress is increased. As shown by Castellanza & Nova (2004), during elastic loading the slope of the stress path is directly linked to Poisson's ratio. Maccarini (1987) measured  $K_0$  as low as 0.1 within the elastic domain, corresponding to a Poisson's ratio of 0.09. At higher stresses, the same author

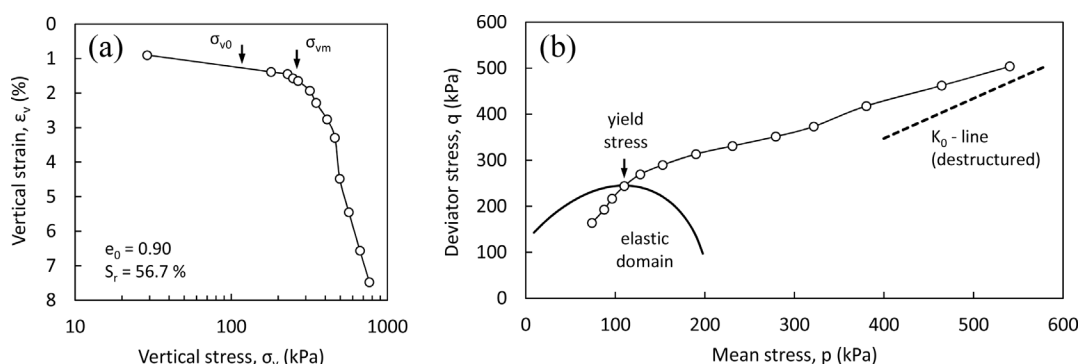


**Figure 1.**  $K_0$  compression test on gneissic residual soil. Adapted from Maccarini (1980, 1987).

reported values of  $K_0$  6 or 7 times greater, compatible with the destructured soil. It should be noted that Maccarini (1980, 1987) measured  $K_0$  in terms of stress increments, i.e.  $K_0 = \Delta\sigma_3/\Delta\sigma_1$ , following the definition given by Andrawes and El-Sohby (1973).

Shearing tests on residual soil give plots of the general shape showed in Figure 2, where data from a series of direct shear tests performed by Escalaya (2016) on young granitic residual soil from Duque de Caxias, Rio de Janeiro, are presented. Intact (undisturbed) samples tested in the direct shear apparatus were first sheared in submerged condition to obtain the peak shear strength. Afterwards, the residual strength was determined using the polished cut-plane technique as described by Garga and Seraphim (1975).

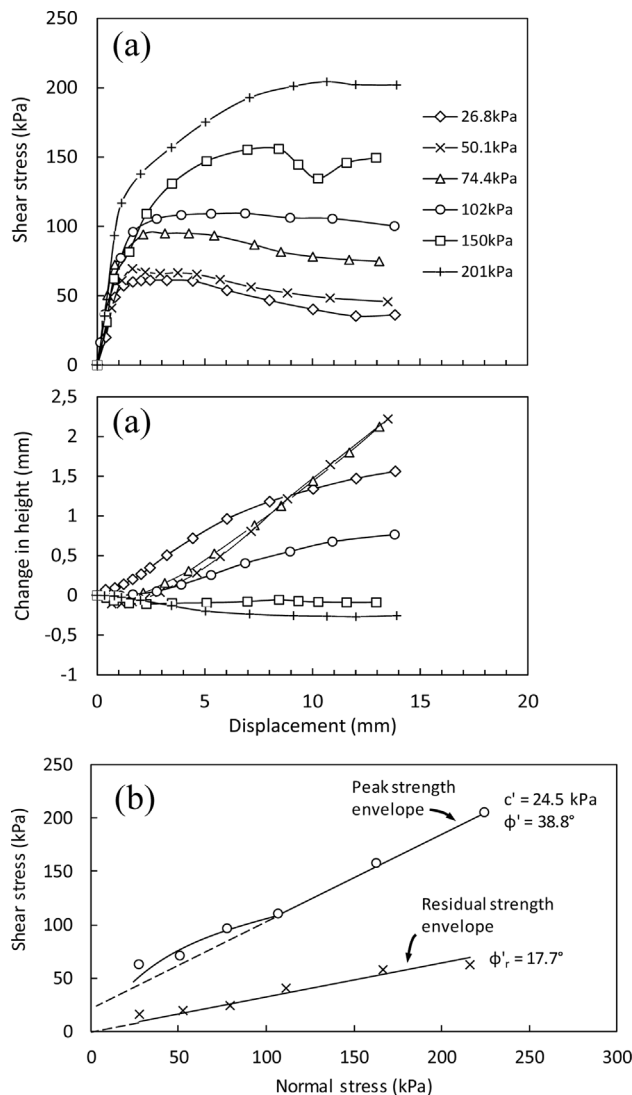


**Figure 2.** Drained direct shear test on granite saprolitic soil from Duque de Caxias, Rio de Janeiro (after Escalaya, 2016). (a) Stress-displacement curves. (b) Peak and residual strength envelopes.

Results from drained shear tests on residual soil reveal that the shear strength parameters are related to the weathering grade, to the mineralogical content and the macrofabric resulting from weathering of the parent rock (Garga, 1988; Massey et al., 1989; Lacerda, 2010). The behavior is similar to that of a dense sand, yet with less pronounced peak strength at low normal stress. The displacement at failure increases with increasing the applied normal stress and, as shown in Figure 2(a), there is a clear reduction in dilatancy as the normal stress is increased. The gradual loss of strength after peak point is passed may be attributed to a gradual decrease in interlocking and destructuration.

The failure envelopes are shown in Figure 2(b). High mica content in mineralogical composition may explain the significant drop in shear strength between peak and residual condition. The residual shear strength envelope, although passing through the axis origin, is not linear at low vertical stress. At a first approximation, a linear envelope with no cohesion intercept has been assumed in Figure 2(b). The peak strength envelope is markedly curved at lower normal stresses. Adopting a linear strength envelope from tests run at high stresses underestimates the strengths in the low stress range (Brand, 1985). Some authors (Massey et al., 1989; Gan & Fredlund, 1996) attribute this additional strength to dilation and weak bonding derived from weathering. Volume increases which are taking place at failure cause somewhat greater values of shearing strength along the curved portion of the envelope, whereas volume decrease takes place along the straight line portion of the envelope. For the case under consideration, the deviation from a straight line occurs at normal stress of about 100 kPa. This point is often referred as the “critical normal stress” that marks the transition from dilatant to contractant behavior during shear.

Figure 3 shows the result of a set of standard drained triaxial tests performed by De Oliveira (2000) on intact young residual soil derived from biotite-gneiss, collected in Alto Leblon, a neighbourhood in the city of Rio de Janeiro. Specimens were isotropically consolidated to effective stresses of 25, 70 and 150 kPa, and then sheared at constant axial strain rate equal to  $8.2 \times 10^{-5} \text{ mm/s}$ . It is possible to identify a general trend in the stress-strain behavior under different confining stresses:

- a) at low confining pressure, after reaching a well defined peak deviator stress at an axial strain less than 3 %, the specimens exhibits brittle failure associated with dilatant behavior. Softening occurs until a stable deviator stress is reached. Additionally, the lower the confining pressure the more dilatant is the behaviour.
- b) at the highest confining pressure, equal to 150 kPa, no peak stress is observed. The stress-strain curve resembles that for an elastic-perfectly plastic material. However, the soil still exhibits the tendency to dilate at failure.

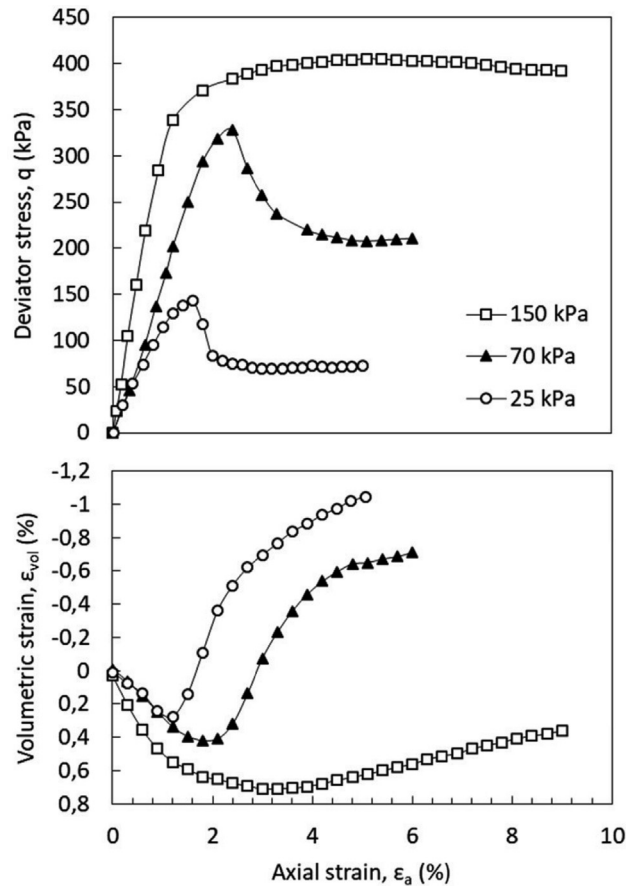


**Figure 3.** Drained triaxial compression test on intact young residual soil derived from biotite-gneiss. Adapted from De Oliveira (2000).

According to De Oliveira (2000), such behavior is typical of soils with bonded structure in the sense described by Leroueil & Vaughan (1990): at low confining stress, peak strength is due to structure, yield is abrupt and the material very brittle; as the confining pressure is increased, the behavior changes from brittle to ductile. De Oliveira (2000) attributed the presence of natural bonding agents between particles to the precipitation of iron oxides between quartz, feldspar and garnet.

Behavior in drained triaxial compression may also follow the trend shown in Figure 4, which is quite different from the one presented in Figure 3. Data are taken from Reis (2004), who tested a gneissic young residual soil from the city of Viçosa, Minas Gerais State, under confining effective stresses ranging from 50 to 400 kPa and obeying the natural banding inclination. The resulting stress-strain curves exhibited less marked peaks and a gradual change from dilatant to contractive behavior with increasing confining stress, which also increased the axial strain at peak. Remarkable was the fact that at the highest confining stress, the soil contracted reaching a peak stress and then it softened at constant volume. This behavior can be explained considering destructuration during the shearing phase,

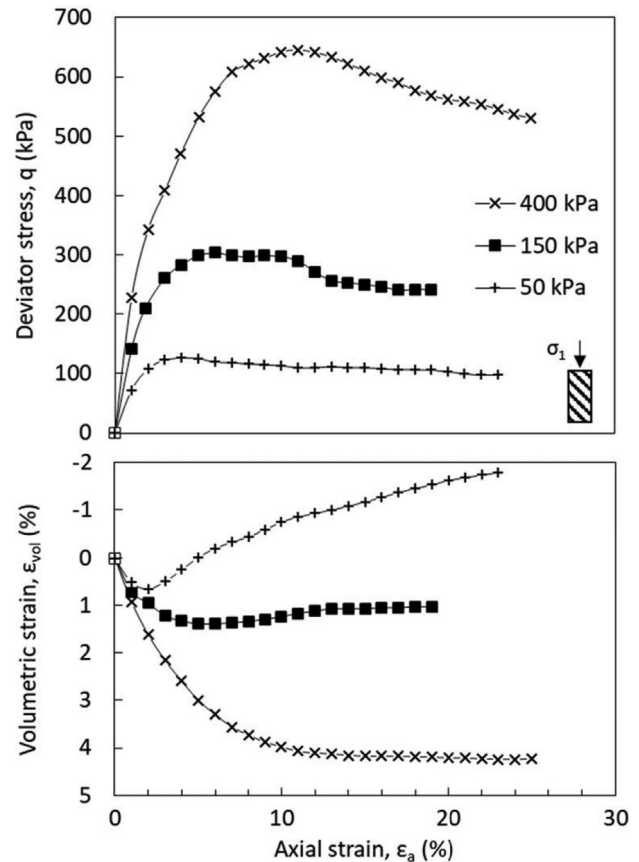


**Figure 4.** Drained triaxial compression test on young residual soil from gneiss with bands oriented as in the field. Adapted from Reis (2004).

which implies shear strength degradation. Similar results have been presented by Santos et al. (2020), who attributed this kind of behavior to the structure inherited from the parent rock. According to them, the observed peak strength should be attributed to the structural effects, as there is no geological evidence of past overconsolidation in this soil.

Other experimental evidences for the existence of bonded structure in residual soils were given by Consoli et al. (1998). They have shown that prestressing a soil sample produces substantial damage to the bonds, deteriorating its strength and stiffness. According to them, this experimental evidence contrasts with ordinary patterns observed on clay, for which overconsolidation has a positive impact on strength and stiffness.

### 3. Constitutive model formulation - mathematical treatment of soil behavior

In the proposed model the irreversible strains are decomposed into two parts, namely the strains resulting from the rearrangement of the grains (plastic strains) and those resulting from damage of structure (collapse strains). Therefore, the total strain rate is decomposed into elastic, plastic and collapse components:

$$\dot{\epsilon}_{ij} = \dot{\epsilon}_{ij}^e + \dot{\epsilon}_{ij}^p + \frac{1}{3} \delta_{ij} \dot{\epsilon}_v^c \quad (1)$$

where  $\delta_{ij}$  is the Kronecker delta. The additive strain decomposition holds under the small strain hypothesis. The elastic strains are, by definition, recoverable and uniquely related to stresses by Hooke's law. Irrecoverable strains are decoupled into those resulting from plastic deformation of the granular matrix,  $\dot{\epsilon}_{ij}^p$ , and those resulting from volume change due to structure collapse,  $\dot{\epsilon}_v^c$ . Both are calculated according to the classical theory of plasticity by assuming the existence of a yield criterion and a flow rule.

The decomposition of irreversible strains into two parts (plastic collapse strain and plastic expansive strain) is not novel in constitutive modeling. As instance, Lade (1977) used distinct yield surfaces and flow rules to calculate plastic and collapse strains in modeling the behavior of Sacramento River Sand.

Within the framework of modeling the behavior of residual soils, the collapse strains are assumed as the volumetric contraction caused by structure degradation. On the other hand, the plastic strains are associated uniquely to grain rearrangement as described by Chandler (1985).

A suitable stress space to describe the triaxial stress state is  $(p', q)$ , where  $p' = (\sigma'_1 + 2\sigma'_3)/3$  is the effective mean stress and  $q = \sigma'_1 - \sigma'_3$  is the deviator stress. The corresponding strain invariants are  $\epsilon_v = \epsilon_1 + 2\epsilon_3$ , the volumetric strain, and  $\epsilon_d = 2/3 * (\epsilon_1 - \epsilon_3)$ , the deviatoric strain. Furthermore, the ratio between the deviator and effective mean stress,  $\eta' = q/p'$ , is very useful in calculations and is referred to as the stress ratio. For simplicity, only saturated behavior is considered, being the aim of the model to reproduce the soil response under drained and undrained triaxial compression.

The assumed expression to describe a teardrop shaped yield locus for a residual soil is:

$$f: \left(\frac{p'}{p_0}\right)^2 + \left(\frac{\eta'}{\eta_0}\right)^2 = 1 \quad (2)$$

Figure 5 shows that the model has a single yield function with two portions clearly distinguishable: the compression cap and the shear failure envelope. The transition between the two parts is smooth and occurs at  $\eta' = \eta_0/\sqrt{2}$ . The parameter  $p_0$  controls the position of the cap, while  $\eta_0$  is the maximum stress ratio associated to shear failure. They are treated as hardening parameters and both depend on irrecoverable strains.

To develop simple and suitable hardening laws to describe the evolution of the yield surface during loading, the following assumptions are introduced:

1. when soil is loaded under isotropic compression, the irreversible volume strain is only caused by structure collapse. In this sense, the cap hardening depends solely on collapse strains resulting from yielding of soil structure, i.e.  $p_0 = p_0(\epsilon_v^c)$ .
2. the shear failure envelope is related to frictional strength and grain rearrangement and, consequently, to plastic strains, i.e.  $\eta_0 = \eta_0(\epsilon_{ij}^p)$ .

The dependence on  $p_0$  of the collapse volumetric strain can be derived by assuming convenient expressions for the calculation of total and elastic volumetric strain increments in isotropic loading. The elastic volumetric response associated with changes in mean effective stress may be described by an equation in the form:

$$e = e_k - \kappa \ln p' \quad (3)$$

where  $e_k$  is the intercept of the unloading-reloading line at  $p = 1$  and  $\kappa$  is its slope in the  $e - \ln p'$  plot. Equation 3 is a common description of soil elastic behavior and provides the shape of the unloading-reloading lines in the  $(e, p')$  plane for stress states within the elastic domain.

For loading beyond the elastic threshold, it is assumed that the reduction in void ratio is directly propor-

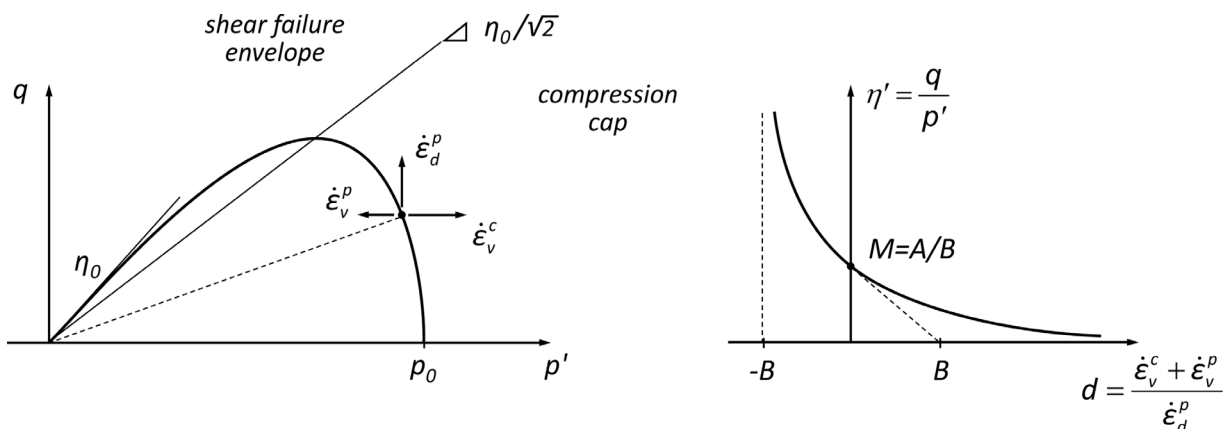


Figure 5. Yield surface, flow vectors and stress-dilatancy relationship.

tional to the void ratio itself and the increase in mean effective stress:

$$de = -\frac{e}{C_b} dp' \quad (4)$$

in which a constant of proportionality,  $C_b$ , has been introduced. Such constant has the dimension of a stress. It has the role of a stiffness and will be referred herein as the “compression modulus”. Equation 4 may also be regarded as the constitutive law for hydrostatic compaction. It states that the compressibility,  $\beta = d\varepsilon_v/dp'$ , is proportional to the current porosity,  $\phi = e/(1 + e)$ . Indeed, dividing both sides of Equation 4 by  $1 + e$  and recalling that  $d\varepsilon_v = -de/(1 + e)$ , one obtains:

$$\frac{d\varepsilon_v}{dp'} = \frac{\phi}{C_b} \quad (5)$$

It is worth noting that this result is valid under the hypothesis of incompressible solids ( $dV_s = 0$ ). Equations 4 and 5 are both written in incremental form and are formally identical. Equation 4 can be easily integrated to obtain the equation for the normal compression line:

$$e = e_0 \exp\left(-\frac{p' - p_0}{C_b}\right) \quad (6)$$

that provides a simple description of the shape of the normal compression line, in the  $(e, p')$  compression plane, accounting for non-linearity of stress-strain response under applied isotropic compression.

The cap hardening law arises from assumption 1. If plastic volumetric strain are neglected in isotropic compression, then the total volumetric strain resulting from the change in  $p_0$  is just elastic and collapse:

$$d\varepsilon_v = d\varepsilon_v^e + d\varepsilon_v^c \quad (7)$$

recalling Equations 3 and 4, it yields

$$\frac{e}{1+e} \frac{dp_0}{C_b} = \frac{\kappa}{1+e} \frac{dp_0}{p_0} + d\varepsilon_v^c \quad (8)$$

from which the cap hardening law is derived:

$$\frac{dp_0}{d\varepsilon_v^c} = \frac{p_0}{\lambda' - \kappa'} \quad (9)$$

with  $\lambda' = \frac{e}{1+e} \frac{dp_0}{C_b}$  and  $\kappa' = \frac{\kappa}{1+e}$

where  $\lambda'$  is the slope of the normal compression line and  $\kappa'$  that of the unloading-reloading line in the  $(\varepsilon_v, \ln p')$  plane. It is worth noting that  $e, p_0$  and, therefore,  $\lambda'$  change as the soil undergoes volumetric deformation.

As introduced in Equation 1, plastic deviatoric strains are assumed to derive from rearrangement of the grains and, thus, are related to grain alignment on a possible slip

surface. This latter mechanism is responsible for decreasing the shear strength and will be modeled as an exponential decay of the maximum stress ratio with plastic deviatoric strain:

$$\frac{d\eta_0}{d\varepsilon_d^p} = -B_q (\eta_0 - \eta_r) \quad (10)$$

where  $B_q$  is the stress ratio decay rate,  $\eta_r$  is a reference value and  $\eta_0$  tends asymptotically to it at failure. Equation 10 is the hardening law of the shear failure envelope.

In general, inelastic flow is not normal to the yield surface. This means that the flow rule is non-associated. Plastic strains are derived from a plastic potential, whereas volumetric collapse is derived from a collapse potential. The flow rule is:

$$\begin{aligned} \dot{\varepsilon}_v^p &= \dot{\lambda} \frac{\partial g}{\partial p'} = -\dot{\lambda} B \eta' \\ \dot{\varepsilon}_d^p &= \dot{\lambda} \frac{\partial g}{\partial q} = \dot{\lambda} \eta' \\ \dot{\varepsilon}_v^c &= \dot{\lambda} \frac{\partial g^c}{\partial p'} = \dot{\lambda} A \end{aligned} \quad (11)$$

where  $\dot{\lambda}$  is the plastic multiplier,  $\eta'$  is the stress ratio,  $A$  and  $B$  are parameters of the model. Following Chandler (1985), the rate of plastic volumetric change resulting from grains rearrangement is assumed to be proportional to the plastic deviatoric rate by a factor,  $B$ , that is a generalization of the angle of dilatancy. In other words, the plastic volumetric strain rate is the expansion necessary for shearing distortion; conversely, the volume collapse is, by definition, the volume contraction due to bonds breakage and mechanical damage. With such a separation, the proposed model has two mechanisms and one criterion (2MIC) according to Chaboche's (2008) classification.

The stress-dilatancy relationship corresponding to Equations 11 is:

$$d = \frac{\dot{\varepsilon}_v^e + \dot{\varepsilon}_v^p}{\dot{\varepsilon}_d^p} = \frac{A - B\eta'}{\eta'} \quad (12)$$

that indicates no irreversible volume change at  $\eta' = A/B$ , that is the so-called “critical state”. Hence, the parameters  $A$  and  $B$  characterize dilatancy, structure collapse and critical state.

The plastic multiplier, for a given stress increment, is derived according to the consistency condition,  $\dot{f} = 0$ . From Equation 2, the differential form of the yield function is:

$$\dot{f} = 0 = \frac{\partial f}{\partial p'} \dot{p}' + \frac{\partial f}{\partial q} \dot{q} + \frac{\partial f}{\partial p_0} \dot{p}_0 + \frac{\partial f}{\partial \eta_0} \dot{\eta}_0 \quad (13)$$

which combined with Equations 9, 10 and 11, gives the expression for the plastic multiplier:

$$\dot{\lambda} = \frac{1}{H} \left( \frac{\partial f}{\partial p'} \dot{p}' + \frac{\partial f}{\partial q} \dot{q} \right) \quad (14)$$

where  $H$  is the hardening modulus:

$$H = - \left( \frac{\partial f}{\partial p_0} \frac{\partial p_0}{\partial \varepsilon_v^c} \frac{\partial g^c}{\partial p'} + \frac{\partial f}{\partial \eta_0} \frac{\partial \eta_0}{\partial \varepsilon_d^p} \frac{\partial g}{\partial q} \right) \quad (15)$$

The overall value of  $H$  depends on two competing terms, each one related to a different mechanism: the first term is linked to volumetric collapse, the second to deviatoric plastic strains.

#### 4. Summary of model parameters - their physical meaning and experimental determination

##### 4.1 Elastic constants

The parameter  $\kappa$ , the so-called “swelling index”, coincides with the slope of the unloading-reloading line in the  $(e, \ln p')$  plot. It can be determined with an isotropic compression test performing unloading-reloading cycles.

The Poisson’s ratio relates the bulk modulus,  $K$ , with the shear modulus,  $G$ , according to the following expression:

$$\frac{G}{K} = \frac{3(1-2\nu)}{2(1+\nu)} \quad (16)$$

The ratio  $G/K$  coincides with the gradient of the volume change curve for a conventional drained compression test (Wood, 1990) if the confining pressure is below the in-situ preconsolidation pressure.

##### 4.2 Inelastic flow

The parameters  $A$  and  $B$  control the inelastic flow. They can be determined using the expression for the stress-dilatancy relationship given in Equation 12. Figure 6 shows the dilatancy ratio  $(d\varepsilon_{vol}/d\varepsilon_{dev})$  obtained from drained triaxial compression tests under different confining stresses plotted against the stress ratio  $(q/p')$ . Data points were derived from total strain increments. For this reason, the initial branch of the stress-dilatancy curve is strongly affected by elastic strains and is not recommended for calibration. Data points taken from the final branch should be favored because they lie on (or are closer to) the critical state. The intercept with the vertical axis corresponds to  $M = A/B = 1.32$ , denoting the critical state. In the present analysis,  $B$  was taken equal to  $M$ , giving a satisfactory description of the stress-dilatancy relationship. The value of parameter  $A$  is the result of the estimation of  $M$  and  $B$ . Therefore, the selected values are of  $A = 1.74$  and  $B = 1.32$ .

The influence of the parameters  $A$  and  $B$  on the predicted response for a drained triaxial test is shown in Figure 7. The results can be summarized as follows. Increasing  $B$  shifts the volume change curve upwards, so greater vol-

ume dilation is predicted. Higher and sharper peaks also occur in the stress-strain curve. Conversely, lowering  $B$  increases the volume contraction and reduces the peak strength. Since calculations were made with constant  $M$ , the ultimate strength is not affected.

##### 4.3 Volumetric hardening

The volumetric hardening law is calibrated by means of an isotropic compression test. Taking logarithms of both sides in Equation 6, a linear relationship is predicted between the mean effective stress and the logarithm of void ratio:

$$p' = p_0 - C_b \ln \left( \frac{e}{e_0} \right) \quad (17)$$

Therefore, the compression modulus,  $C_b$ , equals the slope of the straight line obtained from experimental data if  $\ln e$  is plotted against  $p'$ , as indicated in Figure 8.

The estimation of the preconsolidation pressure should not follow conventional graphical methods, such as the Casagrande’s method. Several authors (Vargas, 1953; Vaughan et al., 1988; Wesley, 1990) questioned the validity of those “conventional” approaches arguing that they were not conceived for residual soils, for which the common definition of “preconsolidation” pressure should not be applied because they do not undergo loading-unloading processes in their formation.

Imposing the continuity of the gradient along the compression curve may be an alternative method to estimate the preconsolidation pressure. If it is assumed that at elastic threshold the unloading-reloading line and the normal compression line have the same slope, one obtains:

$$\frac{\kappa}{p_0} = \frac{e_0}{C_b} \quad (18)$$

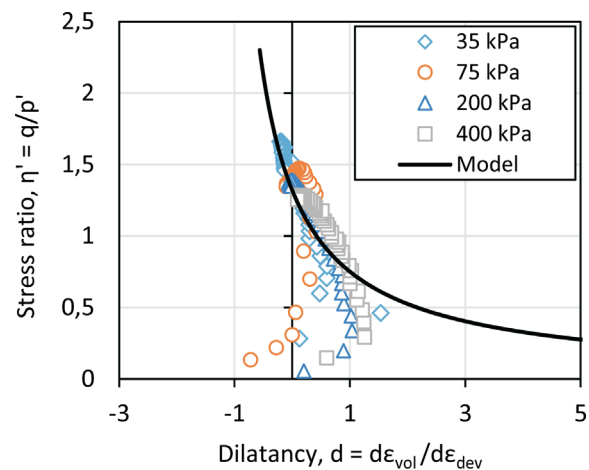


**Figure 6.** Determination of model parameters  $A = 1.74$  and  $B = 1.32$  from the stress-dilatancy relationship of Ouro Preto residual soil.

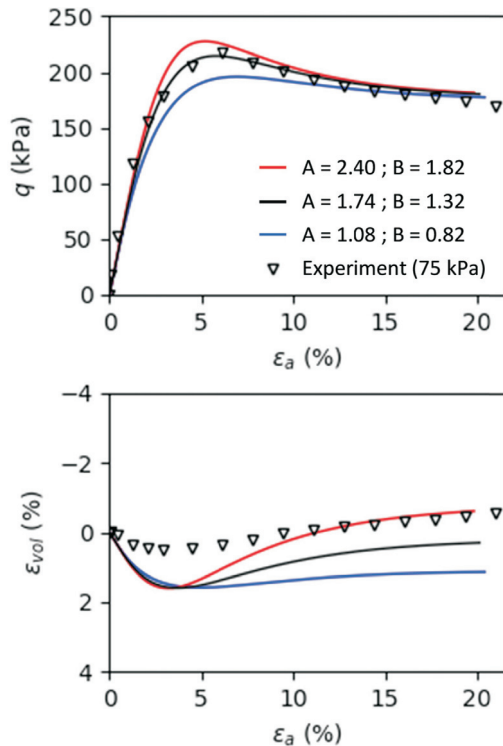
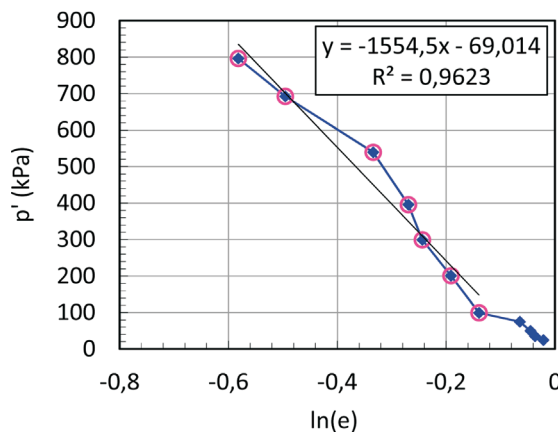


**Figure 7.** Effect of parametric variation on comparison of model simulations and experimental results for drained triaxial compression under 75 kPa of confining pressure.

from which the in-situ  $p_0$  is easily found, known the swelling index,  $\kappa$ , the in-situ void ratio,  $e_0$ , and the compression modulus  $C_b$ .

#### 4.4 Deviatoric softening

The softening rule is a function of plastic deviatoric strains and is calibrated along the post-peak portion of the stress-strain curve for a drained triaxial compression test conducted at low confining pressure.



From Equation 10, it is clear that the relationship between  $\ln(\eta' - M)$  and  $\epsilon_d^p$  is linear, being the parameter  $B_q$  equal to the slope of straight line that best fits the experimental data. The diagram of Figure 9 is obtained using data taken from post-peak branch of the stress-strain curves of the drained triaxial compression tests conducted at low confining pressures. Results clearly suggest that  $B_q$  depends on the effective confining stress. However, for simplicity,  $B_q$  is taken as constant and equal to the average of the slopes.

A general indication of the influence of the value of  $B_q$  on the response in the conventional drained triaxial compression test is shown in Figure 10. Increasing  $B_q$  increases the rate of deviatoric softening, so the stress-strain relationship shows a lower peak strength and the critical state is quickly reached. On the other hand, when  $B_q$  is small, a more ductile behavior is predicted and the model shows higher shear strength. Moreover, the model needs larger deformations to reach the critical state, the volumetric response is strongly affected and the behavior is much more dilatative.

### 5. Model predictions and comparison with experimental results

The model has been employed for predicting the triaxial behavior of Ouro Preto residual soil in drained and undrained conditions. The experimental data have been provided by Futai (2002), who performed isotropic consolidation, consolidated-drained and undrained triaxial compression tests at different cell pressures. Futai et al. (2004) described the testing procedure in detail. The measured stress-strain curves, strain paths and pore pressures responses are presented in the following along with predictions from the present model.

The value of the parameters for Ouro Preto residual soil have been determined from consolidated-drained triaxial compression tests. They are listed in Table 1. A python

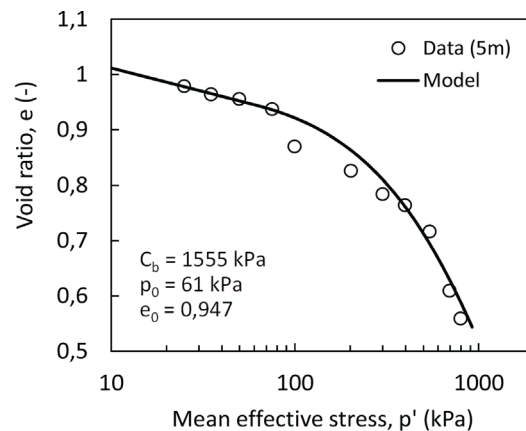


**Figure 8.** Calibration of compression modulus and comparison with experimental results for Ouro Preto residual soil. Data points are taken from triaxial experiments at the end of isotropic consolidation stage.

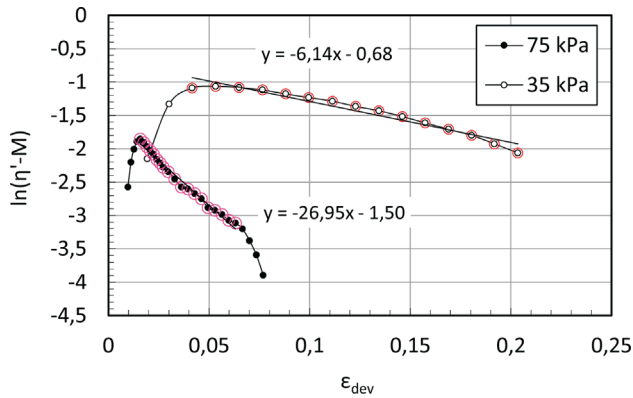


**Figure 9.** Calibration of softening rule with post-peak responses from drained triaxial tests conducted at low confining pressures.

**Table 1.** Summary of parameter values for Ouro Preto residual soil.

Model component	Parameters
Elastic behavior	$\kappa' = 0.018$ $\nu' = 0.15$
Hardening parameters	$p_0 = 61 \text{ kPa}$ $\eta_0 = 1.9$
Inelastic flow	$A = 1.74$ $B = 1.32$
Hardening/softening law	$C_b = 1555 \text{ kPa}$ $e_0 = 0.947$ $B_q = 16.5$

code was developed to integrate the constitutive relations using a semi-implicit algorithm.

The results of the drained triaxial tests are shown in Figure 11(a), together with the predictions of the model. Points indicate the measured soil behavior and solid lines are model predictions. The comparison shows a good agreement between the predicted behavior and the experimental observations. The model is able to predict satisfactorily the stress-strain curves, including the gradual change from dilative to contractive behavior, accompanied by a more ductile response, when confining stress is increased. However, the model overpredicts the volume contraction in the beginning of the loading; a drawback attributable to the chosen flow rule, which is very basic.

The results of the consolidated undrained triaxial compression tests are compared with the predictions in Figure 11(b). The predicted response is less accurate, but still good. Although the model parameters were calibrated from the results of the drained triaxial tests, the model reflects the particular trend in the undrained behavior, especially for the stress paths (Figure 12) and the pore-pressure response, which are reasonably predicted. The response switches

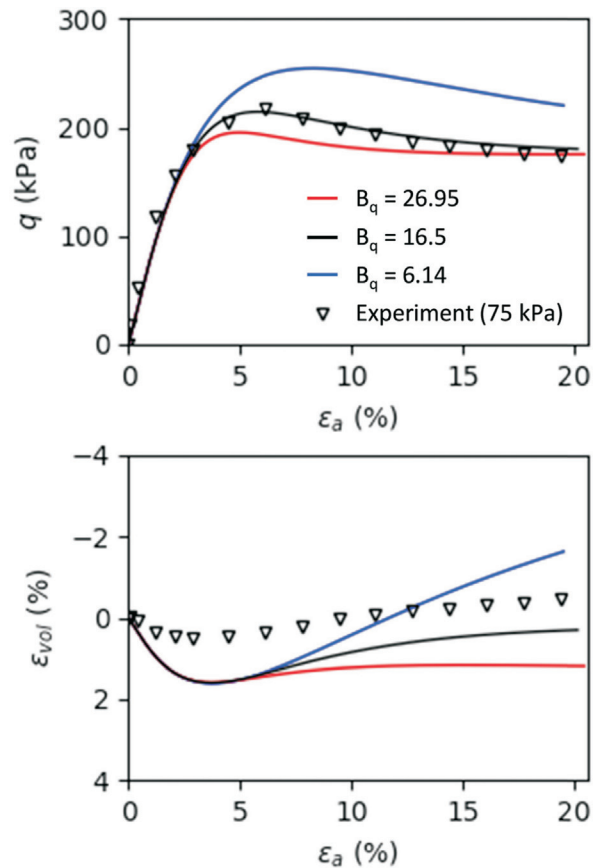


**Figure 10.** Effect of parametric variation on comparison of model simulations and experimental results for drained triaxial compression under 75 kPa of confining pressure.

from initially contractive (increasing pore pressure, decreasing mean effective stress) to dilative (reducing pore pressure, increasing mean effective stress). The rearrangement mechanism is predominant at low confining stress and high stress ratio, so negative pore pressures are consistently predicted for the tests run at 25 kPa and 100 kPa. At higher confining pressures, the dilatancy is suppressed and positive pore pressures are developed. One negative outcome is the stiffer response of the model compared with the test run at 400 kPa of confining pressure.

## 6. Conclusion

A summary of relevant Brazilian experimental work was presented, involving the main geotechnical laboratory tests, in order to address typical patterns of the mechanical behavior of residual soils. The data were used to develop a constitutive model for residual soils based on the assumption that incremental strains consist of elastic, plastic and collapse components. Decomposition of inelastic strains allowed to distinguish the deformations arising from particle rearrangement from those resulting from bonds degradation and particle breakdown. A non-associated flow rule was assumed by adopting two distinct

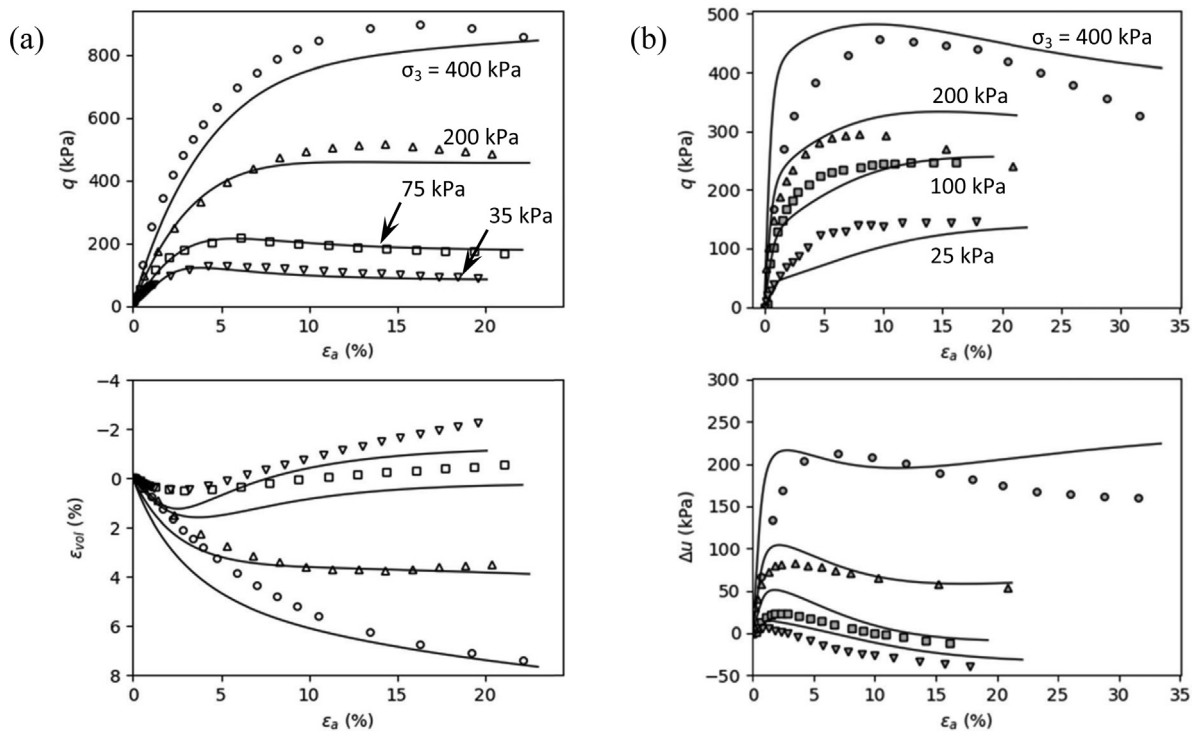


**Figure 11.** Comparison between experimental data from Futai et al. (2004) and model simulations for Ouro Preto residual soil. (a) Consolidated drained triaxial compression tests. (b) Consolidated undrained triaxial compression tests.

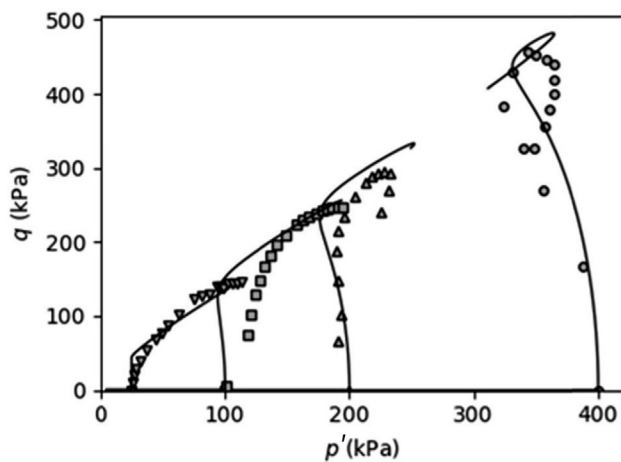


**Figure 12.** Comparison of measured and predicted effective stress paths for consolidated undrained triaxial compression tests on Ouro Preto residual soil.

potential functions, from which each individual inelastic strain was derived. The yield surface, a single continuous function shaped as a teardrop, was expressed in terms of two stress invariants - the mean effective stress and the stress ratio. The hardening laws were developed in order to reproduce the non-linear volumetric response in the  $(e, \ln p')$  plane, under purely isotropic compression, and the softening behaviour associated with shearing strains. The model is characterized by nine parameters that can be de-

termined from simple laboratory tests, such as isotropic compression and conventional consolidated drained triaxial compression tests.

The novel feature of the model is the treatment of bond degradation as a strain-inducing process causing primarily volume contraction. Loss of interlocking is modeled as a softening process related to the particle alignment along a slip plane. The description of those two mechanisms is unified under a single yield criterion. Such an approach is pioneer and some generalizations are still under development.

The model may be enhanced to account for some aspects of the engineering behavior of residual soils that were not included in this work. Possible improvements are: extension to partially saturated states, elastic stiffness degradation with mechanical damage, influence of the third stress invariant, addition of a true cohesion and modeling the anisotropic behavior due to structural discontinuities inherited from the parent rock. In addition, the model should also be tested under loading paths that are more complex than conventional CID and CIU triaxial tests.

The comparison made between published experimental behavior and model predictions is overall acceptable and encouraging. The model was validated in conventional triaxial drained and undrained compression tests by comparing the predicted and observed behavior of Ouro Preto residual soil. In particular, trends in stress-strain, dilatancy and pore pressure behavior, as well as the effective stress

paths were reasonably captured under a wide range of confining stresses.

## Acknowledgments

This study was financed in part by the Coordenação de Aperfeiçoamento de Pessoal de Nível Superior - Brasil (CAPES) - Finance Code 001.

## References

- Andrawes, K.Z., & El-Sohby, M.A. (1973). Factors affecting coefficient of earth pressure  $K_0$ . *Journal of Soil Mechanics and Foundation Engineering Division*, 99 (SM7), 527-539.
- Azevedo, R.F., Reis, R.M., & Vilar, O.M. (2006). Elastoplastic modeling of a young gneiss residual soil in saturated and non-saturated conditions. *Proc. 4th Int. Conference Unsaturated Soils, Carefree*. ASCE, 1968-1979.
- Barata, F.E. (1969). Landslides in the tropical region of Rio de Janeiro. *Proc. 7th Int. Confer. on Soil Mech. and Found. Engng., Mexico City*. ISSMFE, 507-516.
- Blight, G.E. (1989) Design assessment of saprolites and laterites. *Proc. 12th Int. Confer. on Soil Mech. and Found. Engng., Rio de Janeiro*. Vol. 4, Pub. Commit. XII ICSMFE, 2477-2484.
- Bogado, G.O., Reinert, H.O., & Francisca, F.M. (2019). Geotechnical properties of residual soils from the North-east of Argentina. *International Journal of Geotechnical Engineering*, 13(2), 112-121. <https://doi.org/10.1080/19386362.2017.1326682>
- Brand, E.W. (1985) Predicting the performance of residual soil slopes. *Proc. 11th Int. Confer. on Soil Mech. and Found. Engng., San Francisco*, Vol. 5, Pub. Commit. XI ICSMFE, 2541-2578.
- Castellanza, R., & Nova, R. (2004). Oedometric tests on artificially weathered carbonatic soft rocks. *Journal of Geotechnical and Geoenvironmental Engineering*, 130(7), 728-739. [https://doi.org/10.1061/\(ASCE\)1090-0241\(2004\)130:7\(728\)](https://doi.org/10.1061/(ASCE)1090-0241(2004)130:7(728))
- Chaboche, J.L. (2008). A review of some plasticity and viscoplasticity constitutive theories. *International Journal of Plasticity*, 24(10), 1642-1693. <https://doi.org/10.1016/j.ijplas.2008.03.009>
- Chandler, H.W. (1985). A plasticity theory without Drucker's postulate, suitable for granular materials. *Journal of the Mechanics and Physics of Solids*, 33(3), 215-226. [https://doi.org/10.1016/0022-5096\(85\)90012-2](https://doi.org/10.1016/0022-5096(85)90012-2)
- Consoli, N.C., Schnaid, F., & Milititsky, J. (1998). Interpretation of plate load tests on residual soil site. *Journal of Geotechnical and Geoenvironmental Engineering*, 124(9), 857-867. [https://doi.org/10.1061/\(ASCE\)1090-0241\(1998\)124:9\(857\)](https://doi.org/10.1061/(ASCE)1090-0241(1998)124:9(857))
- Costa Filho, L.M., Doebereiner, L., Campos, T.M.P., & Vargas, E. (1989). Fabric and engineering properties of saprolites and laterites. *Proc. 12th Int. Confer. on Soil Mech. and Found. Engng., Rio de Janeiro*. Vol. 4, Pub. Commit. XII ICSMFE, 2463-2476.
- Mello, V.F.B. (1972). Thoughts on soil engineering applicable to residual soils. *Proc. 3rd Southeast Asian Conference on Soil Engineering, Hong Kong*, Southeast Asian Soc. Soil Engng., 5-34.
- Oliveira, C.P. (2000). *Study on the stress-strain-strength behaviour of a saturated biotite-gnaiss residual soil* [Master's dissertation, Pontifical Catholic University of Rio de Janeiro]. Pontifical Catholic University of Rio de Janeiro's repository (in Portuguese). <https://doi.org/10.17771/PUCRio.acad.1788>
- Duarte I.M.R., & Rodrigues C.M.G. (2017) Residual Soils. In *Encyclopedia of Engineering Geology - Encyclopedia of Earth Sciences Series* (pp. 751-752). Springer.
- Escalaya, M.R.A. (2016). *Evaluation of the effect of pore-pressure increase on the strength characteristics of three tropical soils* [Doctoral thesis, Pontifical Catholic University of Rio de Janeiro]. Pontifical Catholic University of Rio de Janeiro's repository (in Portuguese). <https://doi.org/10.17771/PUCRio.acad.30293>
- Fookes, P.G. (1997). *Tropical Residual Soils: A Geological Society Engineering Group Working Party Revised Report*. Geological Society of London.
- Francisca, F.M., & Bogado, G.O. (2019). Weathering effect on the small strains elastic properties of a residual soil. *Geotechnical and Geological Engineering*, 37(5), 4031-4041. <https://doi.org/10.1007/s10706-019-00891-4>
- Futai, M.M. (2002). *Theoretical and experimental study of unsaturated tropical soil behavior: Applied a gully case* [Doctoral thesis, Federal University of Rio de Janeiro]. Federal University of Rio de Janeiro's repository (in Portuguese). <http://www.coc.ufrj.br/pt/teses-de-doutorado/146-2002/925-marcos-massao-futai>
- Futai, M.M., Almeida, M.S.S., & Lacerda, W.A. (2004). Yield, strength and critical state conditions of a tropical saturated soil. *Journal of Geotechnical and Geoenvironmental Engineering*, 130(11), 1169-1179. [https://doi.org/10.1061/\(ASCE\)1090-0241\(2004\)130:11\(1169\)](https://doi.org/10.1061/(ASCE)1090-0241(2004)130:11(1169))
- Futai, M.M., Cecilio, M.O., & Abramento, M. (2012). Shear strength and deformability of residual soils from the Sao Paulo metropolitan area. In *Twin Cities - Soils from Sao Paulo and Curitiba Metropolitan Areas* (pp. 155-188), D'Livros.
- Gan, J.K., & Fredlund, D.G. (1996). Shear strength characteristics of two saprolitic soils. *Canadian Geotechnical Journal*, 33(4), 595-609. <https://doi.org/10.1139/t96-085-307>
- Garga, V.K. (1988). Effect of sample size on shear strength of basaltic residual soils. *Canadian Geotechnical Journal*, 25(3), 478-487. <https://doi.org/10.1139/t88-053>
- Garga, V.K., & Seraphim, L.A. (1975). A note on some observations on a migmatitic residual soil from Rio de Ja-

- neiro. *Soils and Foundations*, 15(4), 1-11. [https://doi.org/10.3208/sandf1972.15.4\\_1](https://doi.org/10.3208/sandf1972.15.4_1)
- Ibañez, J.P. (2008). *Discrete micro-micromechanical modeling of residual soils* [Doctoral thesis, Pontifical Catholic University of Rio de Janeiro]. Pontifical Catholic University of Rio de Janeiro's repository (in Portuguese). <https://doi.org/10.17771/PUCRio.acad.11888>
- Kim, M.K., & Lade, P.V. (1988). Single hardening constitutive model for frictional materials: I. Plastic potential function. *Computers and Geotechnics*, 5(4), 307-324. [https://doi.org/10.1016/0266-352X\(88\)90009-2](https://doi.org/10.1016/0266-352X(88)90009-2)
- Lacerda, W.A. (2010). Shear strength of soils derived from the weathering of granite and gneiss in Brazil. In *Weathering as a Predisposing Factor to Slope Movements* (pp. 167-182). Geological Society of London. <https://doi.org/10.1144/EGSP23>
- Lade, P.V. (1977). Elasto-plastic stress-strain theory for cohesionless soil with curved yield surfaces. *International Journal of Solids and Structures*, 13(11), 1019-1035. [https://doi.org/10.1016/0020-7683\(77\)90073-7](https://doi.org/10.1016/0020-7683(77)90073-7)
- Lade, P.V., & Kim, M.K. (1988). Single hardening constitutive model for frictional materials II. Yield criterion and plastic work contours. *Computers and Geotechnics*, 6(1), 13-29. [https://doi.org/10.1016/0266-352X\(88\)90053-5](https://doi.org/10.1016/0266-352X(88)90053-5)
- Leroueil, S., & Vaughan, P.R. (1990). The general and congruent effects of structure in natural soils and weak rocks. *Géotechnique*, 40(3), 467-488. <https://doi.org/10.1680/geot.1990.40.3.467>
- Maccarini, M. (1980). *Ensaio triaxiais e cisalhamentos direto de um solo residual jovem, derivado de gneisse* [Master's dissertation]. Pontifical Catholic University of Rio de Janeiro (in Portuguese).
- Maccarini, M. (1987). *Laboratory Studies of a weakly bonded artificial soil* [Doctoral thesis, Imperial College London]. Imperial College London's repository. <http://hdl.handle.net/10044/1/8129>
- Martins, F.B., Ferreira, P.M.V., Flores, J.A.A., Bressani, L.A., & Bica, A.V.D. (2005). Interaction between geological and geotechnical investigations of a sandstone residual soil. *Engineering Geology*, 78(1-2), 1-9. <https://doi.org/10.1016/j.enggeo.2004.10.003>
- Massey, J.B., Irfan, T.Y. & Cipullo, A. (1989). The characterization of granitic saprolitic soils. *Proc. 12th International Conference on Soil Mechanics and Foundation Engineering, Rio de Janeiro*. Vol. 6, Publications Committee of XII ICSMFE, 533-542.
- Mendoza, C., Farias, M., & Cunha, R.P. (2014). Validación de modelos constitutivos avanzados de comportamiento mecánico para la arcilla estructurada de Brasilia. *Obras y Proyectos*, 15, 52-70. <http://dx.doi.org/10.4067/S0718-28132014000100005>
- Mendoza, C., & Farias, M. (2020). Critical state model for structured soil. *Journal of Rock Mechanics and Geotechnical Engineering*, 12(3), 630-641. <https://doi.org/10.1016/j.jrmge.2019.12.006>
- Puppi, R.F.K., Hecke, M.B., & Romanel, C. (2018). MCC Hyperplastic constitutive model with coupled damage applied to structured soils. *Geotecnia*, 142, 35-61 (in Portuguese). <http://dx.doi.org/10.24849/j.geot.2018.142.02>
- Reis, R.M. (2004) *Stress-strain behavior of two horizons of a residual soil from gneiss* [Doctoral thesis, University of São Paulo]. University of São Paulo's repository (in Portuguese). <https://www.teses.usp.br/teses/disponiveis/18/18132/tde-06112006-163715/en.php>
- Rocchi, I., & Coop, M.R. (2015). The effects of weathering on the physical and mechanical properties of a granitic saprolite. *Géotechnique*, 65(6), 482-493. <https://doi.org/10.1680/geot.14.P.177>
- Santos, O.F., Lacerda, W.A., & Ehrlich, M. (2020). Effects of cyclic variations of pore pressure on the behaviour of a gneiss residual soil. *Geotechnical and Geological Engineering*, 38, 5201-5212. <https://doi.org/10.1007/s10706-020-01356-9>
- Vargas, M. (1953). Some engineering properties of residual clay soils occurring in Southern Brazil, *Proc. 3rd International Conference on Soil Mechanics and Foundation Engineering, Zurich*. Vol. 1, Publications Committee of III ICSMFE, 67-71.
- Vaughan, P.R., & Kwan, C.W. (1984). Weathering, structure and in situ stress in residual soils. *Géotechnique*, 34(1), 43-59.
- Vaughan, P.R., Maccarini, M., & Mokhtar, S.M. (1988). Indexing the engineering properties of residual soil. *Quarterly Journal of Engineering Geology and Hydrogeology*, 21(1), 69-84.
- Viana da Fonseca, A., & Coutinho, R.Q. (2008). Characterization of residual soils. *Proc. 3rd International Conference Site Characterization, Taipei*. Vol. 1, Taylor & Francis, 195-248.
- Wesley, L.D. (1990). Influence of structure and composition on residual soils. *Journal of Geotechnical Engineering*, 116(4), 589-603. [https://doi.org/10.1061/\(ASCE\)0733-9410\(1990\)116:4\(589\)](https://doi.org/10.1061/(ASCE)0733-9410(1990)116:4(589))
- Wesley, L. (2009). Behaviour and geotechnical properties of residual soils and allophane clays. *Obras y proyectos*, 6, 5-10.
- Wood, D.M. (1990). *Soil Behaviour and Critical State Soil Mechanics*. Cambridge University Press.